A MODEL FOR THE TEAR FILM AND OCULAR SURFACE TEMPERATURE FOR PARTIAL BLINKS

Quan Deng,[1] R. J. Braun,[1,] T. A. Driscoll,[1] & P. E. King-Smith[2]*

[1]*Department of Mathematical Sciences, University of Delaware, Newark, Dwlaware 19711, USA*

[2]*College of Optometry, The Ohio State University, Columbus, Ohio 43210, USA*

[*]*Address all correspondence to R. J. Braun, E-mail: braun@math.udel.edu*

In this paper, we investigate the dynamics of tear film and the associated temperature variation for partial blinks. We investigate the mechanism of fluid supply during partial blink cycles, and compare the film thickness with observation in vivo. We find that varying the thickness of the fluid layer beneath the moving upper lid improves the agreement for the in vivo measurement of tear film thickness after a half blink. By examining the flux of the fluid, we provide an explanation of this assumption. We also investigate the temperature dynamics both at the ocular surface and inside the simulated anterior chamber. Our simulation results suggest that the ocular surface temperature readjusts rapidly to normal temperature distribution after partial blinks.

KEY WORDS: *tear film, blinking, ocular surface temperature, spectral collocation*

1. INTRODUCTION

The ocular tear film is critical for good vision and eye health. The healthy tear film protects the ocular surface with moisture, helps transport waste away from the ocular surface, and provides a smooth optical surface for visual function (Holly and Lemp, 1977). This multilayer film (Mishima, 1965; Ehlers, 1965) has an anterior layer of lipids that is in contact with air that is tens of nanometers thick on average (Norn, 1979; Bron et al., 2004; King-Smith et al., 2009). (Following medical terminology, anterior means the outward direction toward the air, posterior gives the direction into the cornea, inferior is the direction toward the cheek, and superior is the direction toward the moving end of the tear film or forehead). The lipid layer oats upon a primarily aqueous layer (Holly and Lemp, 1977) which is in turn on a mucin-rich region at the corneal surface (Chen et al., 1997; Gipson, 2004; Govindarajan and Gipson, 2010). The precorneal tear film (PCTF) is the tear film located directly on the cornea, while prelens tear film (PLTF) is found on the front surface of a contact lens. For this paper, we focus exclusively on the PCTF.

The PCTF is a total of a few micrometers thick at the center of the cornea after a blink (King-Smith, 2004, 2006; Wang et al., 2003) and has a considerably thicker meniscus (about 0.1 mm or more) around the lid margins where the tear film climbs the wettable part of the eyelids (e.g., Palakuru et al., 2007; Johnson and Murphy, 2006; Harrison et al., 2008). This structure must be reformed rapidly over the blink cycles to enable vision with minimal interruption. The term "blink cycle" is used to mean the combined periods of a single blink, in which the upper lid moves down toward the lower lid and returns, together with the interblink period separating two blinks. Depending on whether the upper lid meets the lower lid by the end of the blink cycle, blink is further characterized as "full blink" or "partial blink."

Blink rate measures the frequency of tear redistribution and is an indicator of the health and proper function of the eye. The blink rates vary among individuals or for the same individual according to various conditions such as age, ocular surface health, or mental focus (Himebaugh et al., 2009; Cruz et al., 2011). Though blink rates can vary between 2–3 blinks/min up to 20–30 blinks/min, a typical blink rate is about 12–20 blinks/min when the subject is at rest under a neutral environment condition (Sibony and Evinger, 1992; Freudenthaler et al., 2003; Tsubota, 1998;

NOMENCLATURE

A	Hamaker constant	h_e	thickness of fluid layer underneath the eyelid
Bi	dimensionless Biot number	k	tear film thermal conductivity
D_s	surface diffusivity of surfactant	k_c	corneal thermal conductivity
E	dimensionless evaporation constant	$\tilde{k}$	ratio of tear film to corneal thermal conductivities
G	Stokes number		
$H_{\min}$	minimum film thickness in initial thickness profile	q	flux along film
		r	fraction of evaporated volume compensated
J	dimensionless evaporative mass flux	t	time
K'	nonequilibrium evaporation coefficient	t_{co}	duration of upstroke
		t_{lg}	duration of lacrimal gland flux
$\bar{K}$	dimensionless nonequilibrium coefficient	t_o	duration of interblink
L'	half length of the palpebral fissure	t_{oc}	duration of downstroke
L'_c	corneal thickness	t_p	duration of punctal flux
$\mathcal{L}_m$	latent heat of water vaporization	t_{bc}	duration of a complete blink cycle
M	Marangoni number	$u^{(s)}$	surface velocity of tear film
P_T	inverse of the thermal Péclet number	x	coordinate along the film
Q	fluid flux along film in fixed domain	y	coordinate through the film
Q_{bot}	fluid flux into the domain at the stationary end	$\tilde{y}$	coordinate through eye
		$\tilde{y}_c$	boundary location inside eye
Q_{lg}	fluid flux due to the lacrimal gland		
Q_p	fluid flux due to the puncta	**Greek Symbol**	
Q_{top}	fluid flux into the domain at the moving end	α	dimensional pressure coefficient for evaporation
S	surface tension number	Γ	insoluble surfactant surface concentration evaporative flux
$\tilde{T}$	temperature field inside eye		
T_B	body temperature	δ	dimensionless effect of pressure on evaporation
T_0	temperature at tear film/eye interface		
T'_s	dimensional saturation temperature	ϵ	ratio of characteristic film thickness over half width of open eye
T_∞	far field temperature		
X	lid location	κ_c	thermal diffusivity of cornea
U'	representative interblink speed	λ	fraction of eye left open at maximum closure
d'	characteristic tear film thickness	μ	viscosity of tear fluid
$f_{\text{in}}, f_{\text{out}}$	coefficients for distribution of boundary fluxes	ξ	coordinate along film in x direction
		ρ	density of water
g	gravitational acceleration	ψ	interpolation function for thermal boundary condition
h_0	dimensionless tear thickness at end		

Monster et al., 1978). A blink rate of 12 blinks/min is an average interblink interval of about 5 s without a mental task requiring concentration. Note that since the actual spontaneous blink has about 280 ms duration, the eye is open for roughly 5 s during an interblink interval (Doane, 1980b). For instance, when three partial blinks take place before a complete blink, the tear film over the inferior cornea will be subject to surface tension, inferior punctal drainage and evaporation for about 15 seconds. Without sufficient tear supply and effective tear redistribution, the tear film becomes more prone to rupture.

Partial blinks are not uncommon. For a sample of normal subjects under experimental conditions of watching an educational film, partial blinks were found on average to represent 10% of the total number (Carney and Hill,

1982). In another group of normal subjects, the rate of partial blinking for an unspecified vision task was 20% of the total (Abelson and Holly, 1977). Doane (1980b) used a high-speed camera system to study in detail the eyelid motion dynamics of the human blink, where films were made from a hidden location behind a one-way mirror. In this manner, he recorded normal, unforced (spontaneous) blinks. He observed that as much as 80% of blinks are partial. McMonnies (2001) found that the relative proportion of partial blinks was much higher in patients with inferior punctate keratopathy than in normal subjects. Similarly to the blink rates discussed above, the frequency of partial blinks is also influenced by the task, with computer games or work causing a higher proportion of partial blinking (Himebaugh et al., 2009). There are influences from age and other factors as well (Cruz et al., 2011); to our knowledge, there is no general explanation available for the variation in partial blink rate.

A number of studies of the tear film during the interblink were able to find reasonable break-up times (BUT) for the film. They also found that the minimum thickness was proportional to $t^{-0.45}$ or $t^{-0.46}$ for long times in the "black line" region (Wong et al., 1996; Sharma et al., 1998; Miller et al., 2002; Braun and Fitt, 2003). This name comes from the experimental observation that thinning is most significant along the line-shaped regions near the lid margins, which appears as a dark region when measured with fluorescence techniques (Miller et al., 2002; Nichols et al., 2012). Abelson and Holly (1977) suggested that the partial blinking motion may be responsible for the punctate staining of the inferior corneal epithelium by producing exposure and inadequacies in the tear film. The subject was also investigated by Himebaugh et al. (2009)

We now turn to the tear film fluid properties. A sample of tears combining all of its components is mildly shear thinning (Tiffany, 1991) but weakly elastic (Pandit et al., 1999). Recent measurements by Leiske et al. (2010) of meibomian lipids (meibum) alone from various mammals show that meibum may have significant elasticity at room temperature; they went on to show that the elasticity is very small above $32°C$ (Leiske et al., 2012). The contribution of the lipid layer to the overall rheology and properties of tears at *in vivo* temperatures is yet to be understood. The apparent surface tension of the tear-air interface and other interfacial properties are affected by surface active polar lipids (McCulley and Shine, 1997; Nagyová and Tiffany, 1999) that are thought to occupy the lipid-aqueous interface and to be insoluble in the aqueous layer. The polar lipids can cause upward motion of the tear fluid after a blink (Berger and Corrsin, 1974; Owens and Phillips, 2001). However, the apparent surface tension of tears appears to be affected by more than the presence of polar lipids (Mudgil et al., 2006; Mudgil and Millar, 2008). In this paper, we simplify the action of the lipid layer to that of a limiting case of strong surface activity from an insoluble surfactant that results in the so-called uniform stretching limit (Jones et al., 2005; Braun and King-Smith, 2007; Heryudono et al., 2007).

Theoretical models of tear film dynamics have recently been reviewed by Braun (2012); a brief review is paraphrased here from Braun et al. (2012). The tear film is commonly assumed to be Newtonian, and the underlying substrate (the cornea) is assumed to be flat (Berger and Corrsin, 1974; Braun et al., 2012). Mathematical studies have incorporated a variety of important effects: surface tension (McDonald and Brubaker, 1971; Wong et al., 1996; Sharma et al., 1998; Miller et al., 2002); polar lipid surface concentration gradients causing the Marangoni effect (Berger and Corrsin, 1974; Jones et al., 2005, 2006; Aydemir et al., 2010); evaporation (Braun and Fitt, 2003; Winter et al., 2010; King-Smith et al., 2009); wettability of the corneal surface via van der Waals terms (Zhang et al., 2003, 2004; Winter et al., 2010); motion of the eyelids in one space dimension (Jones et al., 2005, 2006; Aydemir et al., 2010; Braun and King-Smith, 2007; Heryudono et al., 2007; Maki et al., 2008; Jossic et al., 2009; Zubkov et al., 2012); heat transfer posterior to the tear film (Li and Braun, 2012); and the shape of the eye opening (Maki et al., 2009a,b). These effects may all contribute in different regions of the eye and at different times in the blink cycle.

Partial blinks have been studied extensively in the past with models mentioned above. Following the pioneering work of Doane (1980a), King-Smith and coworkers published a series of papers measuring the tear film thickness with interferometry (King-Smith et al., 2000; Nichols et al., 2003; King-Smith, 2004, 2006). A half blink was captured in a high-speed video recording and it showed a distinctive fringe pattern that revealed a valley at the prior stopping location of the upper lid. The thickness variation relative to the minimum thickness found was computed along a vertical line from the captured image and was used extensively to compare against numerical simulations. Jones et al. (2005) hypothesized that there is a pre-existing fluid layer under the tear film during lid motion. Braun and King-Smith (2007) were first to compare the computed film profile with the quantitative tear film thickness measurement. Heryudono et al. (2007) extended their model by considering a realistic lid motion, and compared their simulation

with the measurement. Their work compared well with the experimental data on the inferior side, but not as well on the superior side.

The thermal dynamics of the tear film and ocular surface is another focus of eye research. Efron et al. (1989) found that the average minimum ocular surface temperature (OST) of the cornea, based on 21 subjects, was slightly inferior to the geometric center of the cornea (GCC). They speculated that this was because the lid margins, the skin that is just posterior to the bottom and top eyelashes, heat the eye and the GCC is superior to (above) the geometric center of the palpebral fissure. The temperature of the GCC 2 s after a blink was found to be $34.3 \pm 0.7°$C on average. The horizontal temperature variation across the ocular surface was fit well with a parabola. The temperature increased as the location moved toward the periphery of the cornea, and toward the lid margins; the temperature of the limbus was $0.45°$C higher than at the GCC.

In order to understand the thermal dynamics of the eye, different models have been developed. Scott (1988a,b) developed finite element (FE) models of heat transfer in the eye that were intended to help decide whether radiative heating led to cataracts in glass blowers. Other finite element models of heat transfer in the eye found steady-state OST values within experimental ranges (Ng and Ooi, 2006, 2007). Steady-state finite element models with conductive and convective heat transfer in the aqueous humor have been developed in two (Heys and Barocas, 2002; Ooi and Ng, 2008) and three (Karampatzakis and Samaras, 2010) dimensions with similar conclusions; the location of the minimum OST and the overall heat transfer through the anterior chamber is not significantly affected by the distorted temperature field. Approximate analytical models have been developed as well (Canning et al., 2002; Fitt and Gonzales, 2006). Li and Braun (2012) showed that the minimum model necessary to approximate the surface dynamics of the tear film is substantially less complicated, and a simple rectangular geometry beneath the tear film was sufficient to capture OST dynamics. Their work was restricted to the interblink period only, when both upper and lower lids are stationary. Deng et al. (2013) extended the modeling of tear film over multiple (complete) blink cycles. The numerical results reveal a similarity to quantitative *in vivo* observations of the film dynamics and measured ocular surface temperature. This work also explored the periodicity in the film and temperature dynamics with different flux conditions and end motions.

In this paper, we study the dynamics of half blinks in terms of tear film and ocular surface temperature. The model we develop here is an extension of the model employed by Li and Braun (2012), and the model formulation relies heavily on that work. Evaporation and van der Waals forces are included in the model to give a more realistic description of the tear film dynamics. We will revisit the hypothesis that the thickness of the pre-existing fluid layer remains constant over blink cycles, which is commonly used in existing models for complete blinks, but may no longer be reasonable for partial blinks. We give a brief formulation of the problem in Sec. 2. In Sec. 3 we compare the tear film thickness after a half blink with the measurements in Braun and King-Smith (2007) and Heryudono et al. (2007). We also give the dynamics of temperature field both inside the anterior of the eye (cornea plus aqueous humor) and at the ocular surface for partial blinks. We discuss the simulation results in Sec. 4 and provide model details in the Appendices.

2. FORMULATION

A sketch of the mathematical model for the tear film and cornea temperature is shown in Fig. 1. The coordinate directions (x', y') and velocity components (u', v') are along and perpendicular to, respectively, the flat surface that approximates the corneal surface. We apply lubrication theory to the Navier-Stokes equations and boundary conditions (Oron et al., 1997; Craster and Matar, 2009), and treat heat diffusion in the anterior eye. The approach yields a coupled nondimensionalized system for film thickness h and temperature T. Details of the model derivation are given in Appendix A. The dimensional and nondimensional parameters are listed in Tables 1 and 2.

For film thickness $h(x, t)$, we have the following governing equation:

$$\partial_t h + EJ + \partial_x q = 0, \quad X(t) < x < 1, \quad 0 < t, \tag{1}$$

where fluid flux q along the film and evaporative flux J are given, respectively, by

$$q = \frac{h^3}{12} \partial_x (S \partial_x^2 h + A h^{-3}), \quad \text{and} \tag{2}$$
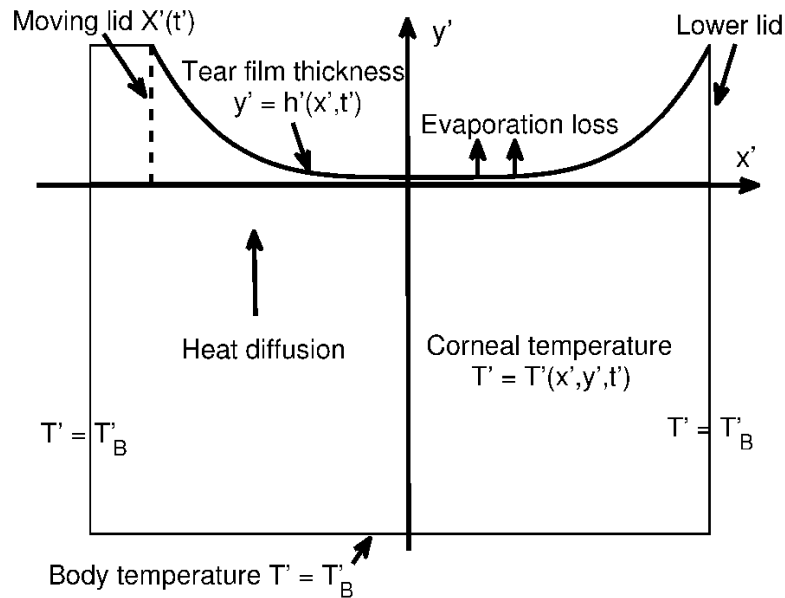
FIG. 1: A sketch of pre-corneal tear film with heat transfer from the cornea indicating important mathematical quantities. The dimensional upper lid location is $X'(t')$; this end moves in blink cycle models.

TABLE 1: Dimensional parameter definitions and values. Unless otherwise noted, these values were used to generate the computational results. κ_c, specific heat of lens instead of water is used. K is chosen to satisfy the experimental thinning rate (4 μm/min) of the tear film thickness due to Nichols et al. (2005). α and A' are recovered from the nondimensional parameters in Winter et al. (2010)

Dimensional parameters		
Parameter	**Description**	**Value**
d'	Characteristic thickness of tear film	5×10^{-6} m
L'	Half length of the palpebral fissure	5×10^{-3} m
L'_c	Corneal thickness	5×10^{-4} m
y'_c	Model depth into eye	$5L'_c$
μ	Viscosity (Tiffany, 1991)	1.3×10^{-3} Pa $\cdot$ s
σ	Surface tension (Nagyová and Tiffany, 1999)	0.045 N $\cdot$ m^{-1}
k	Tear film thermal conductivity (Scott, 1988b) (water)	0.68 W $\cdot$ m$^{-1} \cdot$ K^{-1}
k_c	Corneal thermal conductivity (Scott, 1988b)	0.58 W $\cdot$ m$^{-1} \cdot$ K^{-1}
ρ	Density (water)	10^3 kg $\cdot$ m^{-3}
$\mathcal{L}_m$	Latent heat of vaporization (water)	2.3×10^6 J $\cdot$ kg^{-1}
T'_s	Saturation temperature	$27°$C
T'_B	Body temperature	$37°$C
g	Gravitational acceleration	9.81 m $\cdot$ s^{-1}
κ_c	Thermal diffusivity of cornea (Scott, 1988b)	1.9×10^{-7} m$^2 \cdot$ s^{-1}
A'	Hamaker constant (Winter et al., 2010)	3.5×10^{-19} Pa $\cdot$ m^3
U'	Representative interblink speed	5 mm s^{-1}
α	Pressure coefficient for evaporation (Winter et al., 2010)	3.6×10^{-2} K $\cdot$ Pa^{-1}
K'	Nonequilibrium coefficient (Li and Braun, 2012)	1.5×10^5 K $\cdot$ m$^2 \cdot$ s $\cdot$ kg^{-1}

TABLE 2: Nondimensional parameter definitions and values

Parameter	Definition	Value
ϵ	$\dfrac{d'}{L'}$	10^{-3}
E	$\dfrac{k(T'_B - T'_s)}{d'\mathcal{L}_m \epsilon \rho U'}$	118.3
S	$\dfrac{\sigma \epsilon^3}{\mu U'}$	6.92×10^{-6}
$\overline{K}$	$\dfrac{kK'}{d'\mathcal{L}_m}$	8.9×10^3
h_e	$\dfrac{h'_e}{d'}$	0.4–1.6
δ	$\dfrac{\alpha \mu U'}{\epsilon^2 L(T'_B - T'_s)}$	4.66
A	$\dfrac{A'}{L'd'\mu U'}$	2.14×10^{-6}
$\tilde{k}$	k/k_c	1.17
P_T	$\dfrac{L'\kappa_c}{U'L_c'^2}$	0.76
Bi	$\dfrac{h_c d'}{k}$	0–0.1

$$J = \left[\frac{T_0 + \mathrm{Bi}T_\infty h}{1 + \mathrm{Bi}h} - \delta \left(S\partial_x^2 h + Ah^{-3} \right) \right] \left[\overline{K} + \frac{h}{1 + \mathrm{Bi}h} \right]^{-1}. \tag{3}$$

Here E gives the size of the nondimensional evaporative mass flux J from the film surface, and A is the nondimensional Hamaker constant in the unretarded van der Waals force. S measures the effect of surface tension at the air/tear film interface compared to viscous forces in the film. Representative values of the parameters are given in Table 2. Thus the model includes the evaporative effect from the aqueous layer and the van der Waals-type forces (Ajaev and Homsy, 2001; Ajaev, 2005a) representing the wettable corneal surface. We neglect gravitational effects because it typically acts too slowly compared to the blink and interblink times that we consider here (see Appendix A).

The aqueous component of the tear liquid cannot pass onto the hydrophobic skin cells at the eyelid margin and the liquid is assumed to be pinned along this line. Because of this we prescribe the thickness of the tear film at each end of the fluid domain to be h_0 via

$$h(1, t) = h[X(t), t] = h_0. \tag{4}$$

Here $X(t)$ represents lid motion to be given in Sec. 2.1. We will use $\dot{X}(t)$ to represent lid velocity. The remaining two boundary conditions specify the fluid flux at each end, and they are discussed in Sec. 2.2.

Turning to the rectangular region underneath the tear film, only heat diffusion is considered there; the small effect of fluid motion inside the eye on heat transport (Heys and Barocas, 2002) justifies this assumption. The rectangular model eye region is deep enough to include the cornea and part of the anterior chamber. The temperature T inside the model eye domain is governed by

$$\partial_t T = P_T \left[\left(\frac{L'_c}{L'} \right)^2 \partial_x^2 T + \partial_y^2 T \right]. \tag{5}$$

The length scales L'_c in the y' direction and L' in the x' direction are given in Table 1. P_T is the inverse of the thermal Péclet number and is given in Table 2. On the nonfilm edges of the domain, where $x' = L'$ or $y' = \pm y'_c$, we specify body temperature, $T' = T'_B$.

   The domain for heat transfer and the film domain are connected through a time-dependent boundary condition at $y = 0$ and $X'(t') \le x \le L'$, via applying continuity of temperature and heat flux:

$$\partial_{\tilde{y}} \tilde{T}(x, 0, t) + (1 - \psi) \frac{L'_c \tilde{k}}{h'_e d'}(T_0 - T_B) + \psi \mathrm{Bi}(T_0 - T_\infty) = 0. \tag{6}$$

As illustrated in Fig. 2, we use a function $\psi(x, t)$, given by

$$\psi(x, t) = \frac{1}{2} \left[1 - \tanh \left(\frac{x - X(t)}{x_w} \right) \right], \tag{7}$$

to give a smooth transition between different heat transfer rates from the upper eyelid and the open eye. The denominator is chosen to keep the transition region small compared to the domain size.

2.1 Lid Motion

We divide a blink cycle into upstroke, interblink (open), and downstroke phases. One end of the domain keeps moving to mimic the blinking in the eye, which is described by a mathematical fit to the lid position $X(t)$, and was first obtained by Berke and Mueller (1998). Jones et al. (2005) measured and fit the data during the upstroke of the eyelid and the interblink. Braun and King-Smith (2007) used a sinusoidal lid motion for full blink cycles. Heryudono et al. (2007) developed a lid motion function based on the measurements of Doane (1980b) and Berke and Mueller (1998), which we refer as the realistic lid motion, as shown in Fig. 3 and given, in nondimensional form, by
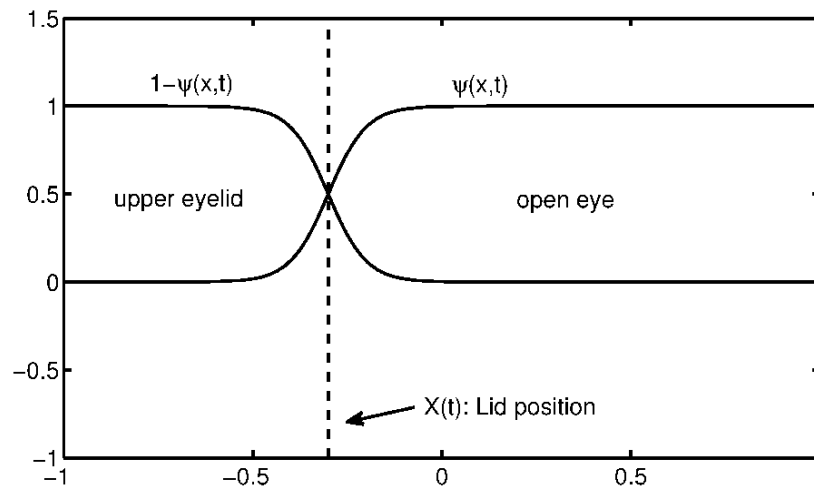
FIG. 2: The Neumann conditions corresponding to open air and upper eyelid can be joined smoothly with a hyperbolic tangent function. The sketch shown uses $x_w = 0.1$ and is not to scale; the width of the transition between the two types of boundary fluxes in our computations is only about 1% of the domain length.
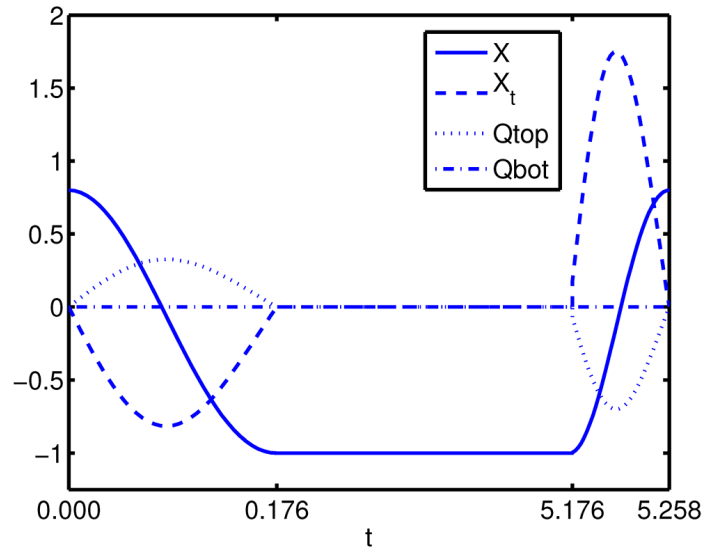
FIG. 3: An illustration of realistic lid motion $X(t)$, lid speed $\dot{X}(t)$, and boundary fluxes Q_{top} and Q_{bot} for a full blink with flux proportional to lid motion (FPLM) boundary condition. (Note that $\dot{X} = X_t$ here). The solid curve represents the lid position $X(t)$ during the blink, which starts and ends slightly off $x = 1$ (lower eyelid), meaning that a fraction λ of the domain remains open to air over multiple blinks. The dashed line gives the corresponding lid velocity $\dot{X}(t)$. The dotted line gives the influx of fluid from the upper eyelid Q_{top} due to our assumption of a pre-existing fluid layer beneath the film (10). The dash-dot line represents the flux of fluid from the lower eyelid Q_{bot}, which will remain zero for the FPLM condition, but will be positive as a result of lacrimal gland supply in the FPLM+ condition used later. Note that the t axis is not to scale.

$$X(t) = \begin{cases} 1 - 2\lambda - 2(1-\lambda)\left(\dfrac{t}{t_{co}}\right)^2 \exp\left[1 - \left(\dfrac{t}{t_{co}}\right)^2\right], & 0 \leq t \leq t_{co} \\[3mm] -1, & t_{co} \leq t \leq t_{co} + t_o \\[3mm] -1 + 2(1-\lambda)\left(\dfrac{t - t_{co} - t_o}{t_{oc}}\right)^2 \exp\left[1 - \left(\dfrac{t - t_{co} - t_o}{t_{oc}}\right)^2\right], & t_{co} + t_o \leq t \leq t_{bc}. \end{cases} \quad (8)$$

Here λ is the fraction of the fully open region that is still open at the end of the downstroke, when the domain is at its smallest. We will follow the approach taken in Braun and King-Smith (2007) and Heryuodono et al. (2007) where we consider $\lambda = 0.1$ as being fully closed, which we refer to as a full blink (Fig. 3). Any blink with $\lambda > 0.1$ will be considered a partial blink. The period of a nondimensionalized complete blink cycle is $t_{bc} = t_{co} + t_o + t_{oc}$, where $t_{co} = 0.176$, $t_o = 5$, and $t_{oc} = 0.082$ represent the duration of the upstroke, interblink, and downstroke, respectively. Thus, a complete blink cycle takes $t_{bc} = 5.258$.

2.2 Flux Conditions

The flux conditions we use attempt to model the flow along the lids during the blink cycle, as described by Doane (1981), by approximating the flow around the lid margins *in vivo* to flux at the ends of a one-dimensional (ID) domain (Jones et al., 2005; Heryuodono et al., 2007):

$$q(X(t), t) = \dot{X}h_0 + Q_{\text{top}}, \quad \text{and} \quad q(X(t), t) = -Q_{\text{bot}}, \quad (9)$$

where h_0 is the tear meniscus width (nondimensionalized), Q_{top} and Q_{bot} represent the fluxes into the domain at the moving end and at the stationary end, respectively. Jones et al. (2005) observed that a significant volume of tear fluid is stored under the upper and lower eyelid, and thus as the lid moves up or down, there is a certain flux of fluid from the under the upper eyelid. They assumed that the layer thickness is a constant h_e', and hence Q_{top} relative to the lid is proportional to the eyelid velocity. We refer to this flux condition as the flux proportional to lid motion, or FPLM, condition. Mathematically, the fluxes at the ends in this case are

$$Q_{\text{top}} = -\dot{X} h_e/2, \quad Q_{\text{bot}} = 0, \tag{10}$$

where $h_e = h_e'/d'$ is the scaled thickness of the fluid layer under the film. The fluxes for the end for a full blink and the FPLM condition are shown in Fig. 3.

In tear film studies, different h_e' have been used in numerical simulations. Jones et al. (2005) used $h_e' = 8.24$ μm based on the estimated tear film thickness under the lower lid by Norn (1966) from pipette sampling; they assumed a characteristic thickness of 10 μm. This is thicker than most experimentally observed film thickness in the range of $3 - 5$μm (King-Smith et al., 2006). Heryudono et al. (2007) used $h_e' = 4$ μm based on the measurements of King-Smith et al. (2006) and the fact that the tear film thickness under the lids is smaller at the margin, as observed in x-ray tomography (Kessing, 1967).

In previous studies, h_e' was assumed to be constant (Jones et al., 2005, 2006; Heryudono et al., 2007; Jossic et al., 2009; Aydemir et al., 2010; Zubkov et al., 2012). However, for partial blinks it may be reasonable to assume that h_e' should decrease over partial blinks, since the amount of fresh tear fluid may be reduced compared to a full blink (Doane, 1981). Further, for partial blinks, the inferior cornea is exposed to the open air longer than its superior counterpart, resulting in a reduced tear film thickness. In Sec. 3, we will assume there is a decrease in h_e' from full blink to partial blink, and explore the film behavior under this assumption.

Maurice (1973) observed significant drainage along the lid margins beginning with the lids about halfway open or so, and ending up to 3 s after the lids have fully opened. It is also believed that the lacrimal gland supplies new tear fluid mostly under the upper lid, and that the new tear fluid can flow around the lid margins (Lorber, 2007; Maurice, 1973; Doane, 1981). To describe these phenomena in a 1D model, Heryudono et al. (2007) proposed the FPLM+ condition to include both lacrimal glands supply and punctal drainage. In this formulation, influx and outflux are both assumed to be Gaussian-shaped functions. The widths of the Gaussian functions are scaled to comply with the experimental observations. Detailed description of the FPLM+ condition and its derivation are given in Appendix B.

2.3 Initial Conditions

We consider two initial volumes $V_0 = 1.576$ and $V_0 = 2.576$ for the open phase. (We use the term volume here, though it is really volume per unit length, or area). The latter comes from estimating the volume for a $d = 5$ μm film with quadratic menisci having width 0.36 mm and thickness $h_0' = 0.065$ mm at both ends (Maki et al., 2008). The former number simulates a reduced tear volume for a 2.5 μm film while the film thicknesses at the ends are the same h_0'. The added volume during the upstroke gives

$$V = \int_0^{t_{co}} Q_{\text{top}} dt = \int_0^{t_{co}} -\dot{X}(h_e/2) dt = -(h_e/2)\left[-1 - (1 - 2\lambda)\right] = h_e(1 - \lambda). \tag{11}$$

We can write our initial volume $V_i = V_0 - V$. The initial condition for the film is specified as

$$h(x, 0) = h_{\min} + (h_0 - h_{\min})\left[1 - 2\frac{1 - x}{1 - X(t)}\right]^m. \tag{12}$$

Here m characterizes the shape of the polynomial and $h_{\min}$ is computed such that the initial volume is the specified value $h(x, 0)$ is V_i. This function smoothly varies from the boundary values to the minimum value and can be used to mimic expected tear film thickness distributions in either the closed or open conditions. The initial temperature field is specified as body temperature:

$$T(x, \tilde{y}, 0) = 1. \tag{13}$$

Deng et al. (2013) developed the initial condition for the blink cycle of interest by simulating a blink or two, then using the data from subsequent blink cycles. This was done because any transients from the original initial condition were eliminated; if periodic solutions existed, they effectively became so after a pair of blink cycles. We will follow this approach in the computation of partial blinks in the next section.

3. RESULTS

In this section, we present results for film thickness and temperature during partial blinks. We begin by discussing experimental results for the thickness, then give computed results, followed by a detailed comparison. We then turn to computed temperature results, and then compare them to published experimental results.

If not otherwise mentioned, parameters used in the computations are $V_0 = 1.576$, $\lambda = 0.5$, $h_0 = 13$.

3.1 Film Thickness

We will compare our simulation with *in vivo* experiments using interferometry (Doane, 1980b; King-Smith et al., 2004, 2006). We choose to compare an example from the PLTF rather than PCTF, as the best contrast between the tear fluid and underlying surface occurs in that case.

Figure 4(a) shows an image of the PLTF immediately after a half blink. The interference fringes shown in the photo indicate a change of 0.16 μm for each change between light and dark fringes. Figure 4(b) shows the film thickness variation along the vertial line shown in Fig. 4(a). Starting from the inferior side (right end), thickness decreases rapidly and reaches a minimum near the center of the image. Then the film thickness increases with a milder slope and leaves a valley behind. Near the superior end (left end), the film thickness drops again. Separated by the valley, there is less fluid captured at the superior side than the inferior side. Note that since the film thickness variations at upper and lower menisci were not captured in the interference fringes, we restrict our comparison to the interior of the eye domain. In the following, the thickness variation shown in Fig. 4(b) was nondimensionalized and shifted along the film length such that the measured minimal film thickness coincides with our numerical simulation.
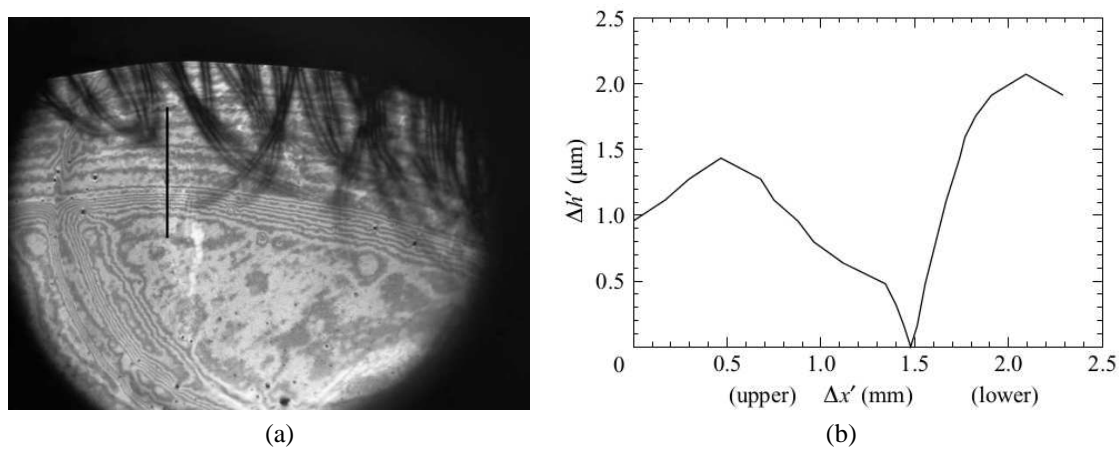
FIG. 4: (a): Interference fringes for the total tear film thickness of the PLTF just after a half blink. The horizontal extent of the image is about 8 mm; the thickness difference between neighboring bright fringes is 0.32 μm. The upper lid descended to the region of compact fringes in the middle of the image and then rose to the open position (upper lashes still visible). The curving feature near the left-hand edge of the illuminated region is the edge of the optic zone of the lens. (b). Dimensional thickness variation relative to the minimum found was computed from the image along the vertical line in the upper left quadrant. Comparison of broad and narrow band contrast leads to an estimated minimum film thickness of 0.48 μm. We will compare a number of results in this paper with this thickness measurement.

Braun and King-Smith (2007) studied the half-blink phenomenon and compared simulation with experiments. By including the realistic lid motion, Heryudono et al. (2007) improved on the sinusoidal lid motion in Braun and King-Smith (2007) and the resulting simulation was able to better capture the valley shown in Fig. 4(b). However, those results had more fluid stored on the superior side of the valley, rather than more on the inferior side of the valley as was seen experimentally. To improve the model to capture these features, we first include evaporation and van der Waals force to describe the tear film dynamics. Instead of having the drainage Q_p balance the lacrimal gland supply Q_{lg} (Heryudono et al., 2007), we compute the drainage by (34) such that the net influx $Q_{lg} - Q_p$ compensates only a fraction r of evaporation loss V_e during the partial blinks. Here we use the parameter f_{in} to specify that the majority of supply from lacrimal glands comes from the upper eyelid. After Heryuodono et al. (2007), we refer to this flux condition as the FPLM+ condition, and give detailed expressions in Appendix B. As mentioned in Sec. 2.3, we will use a full blink to generate an initial condition for later partial blinks. In Fig. 5, we illustrate this approach by showing a half blink following a complete blink. Note that a valley is formed due to the half blink and is shifted toward the superior side following the moving end.

In order to compare with experiment, we restrict attention to the thin film region ($0 < h < 2$), and plot the film for three consecutive half blinks after a full blink, as displayed in Fig. 6. The full blink is used to provide the initial condition for the subsequent half blinks. We observe that valleys are formed for all half blinks. However, we find that the comparison between simulation and experiment is not ideal. In the experimental data, the peak of the bump near the superior side is lower than its counterpart. This suggests that the consideration of evaporative effect and van der Waals force is not adequate to explain the observed tear film distribution.

Here we used $h_e = 1$ for both the complete blink and multiple partial blinks. This suggests that we revisit the assumption that the pre-existing fluid layer under the tear film remains constant over multiple blinks. We note that the tear film on the inferior side of the eye will receive less fluid than the superior side from partial blinks, since effective tear redistribution only takes place during the blinking process. This is illustrated by Fig. 6(b), where it is clear that the flux toward the lower meniscus reduces significantly. As a result, the film on the inferior side thins at a roughly constant rate due to evaporation and less supply of new tear fluid. Thus it is reasonable to assume that h_e will vary from complete blink to partial blink. A simple modification on h_e to reflect this observation is to assume $h_e = 1$ for the full blinks, and $h_e = 0.4$ for subsequent half blinks. The results are shown in Fig. 7. The most noticeable difference can be seen near the upper meniscus, where the bulk of fluid is greatly reduced due to our specification of a thinner fluid layer under the film for partial blinks.

Better agreement with the experimental data is possible by carefully tuning the parameters r, which controls the amount of fluid supply, and f_{in}, which specifies the allocation of fluid supply. Figure 8 shows results for $r = 0.4$ and $f_{in} = 0.8$, which represents more lacrimal gland supply from the upper meniscus than the lower meniscus. The formation of a bump superior to the valley agrees with the experimental observation.

Note the correspondence between the film and the flux shown in Fig. 9 for four time levels at the upstroke. We observe the initial flux barrier caused by local minimum from the downstroke phase. Thus the fluid supply on the superior side accumulates toward this valley, as it cannot be easily transported to the inferior side, resulting in effectively no flux through the valley.

3.2 Temperature

We now turn to the temperature results. We plot temperature contours in the rectangle that represents an idealized part of the anterior eye that contains the cornea and the aqueous humor behind it; we refer to this domain as the "anterior eye" for simplicity. With the same parameters used in Fig. 8, we show temperature contours in the anterior eye for the half blink following a full blink. The tear film is located along the $y = 0$ edge, with the right end of the tear film fixed at $x = 1$ and the left end $X(t)$ moving through the domain. Figure 10(a) shows the temperature at $t = t_{co} + t_o = 5.176$, which is right before the downstroke of the half blink. It can be seen that the temperature has a roughly uniform distribution in the x direction away from the ends of the domain. Figures 10(b)-10(e) show the change of temperature during the blinking process, which takes $t_{oc} + t_{co} = 0.258$ and is shorter than the interblink cycle, which takes $t_o = 5$. Figure 10(e) shows that immediately after the half blink, there exists a temperature variation along the x direction. Figure 10(f) suggests that this nonuniformity will be relaxed within around 1 s after fully opening again.
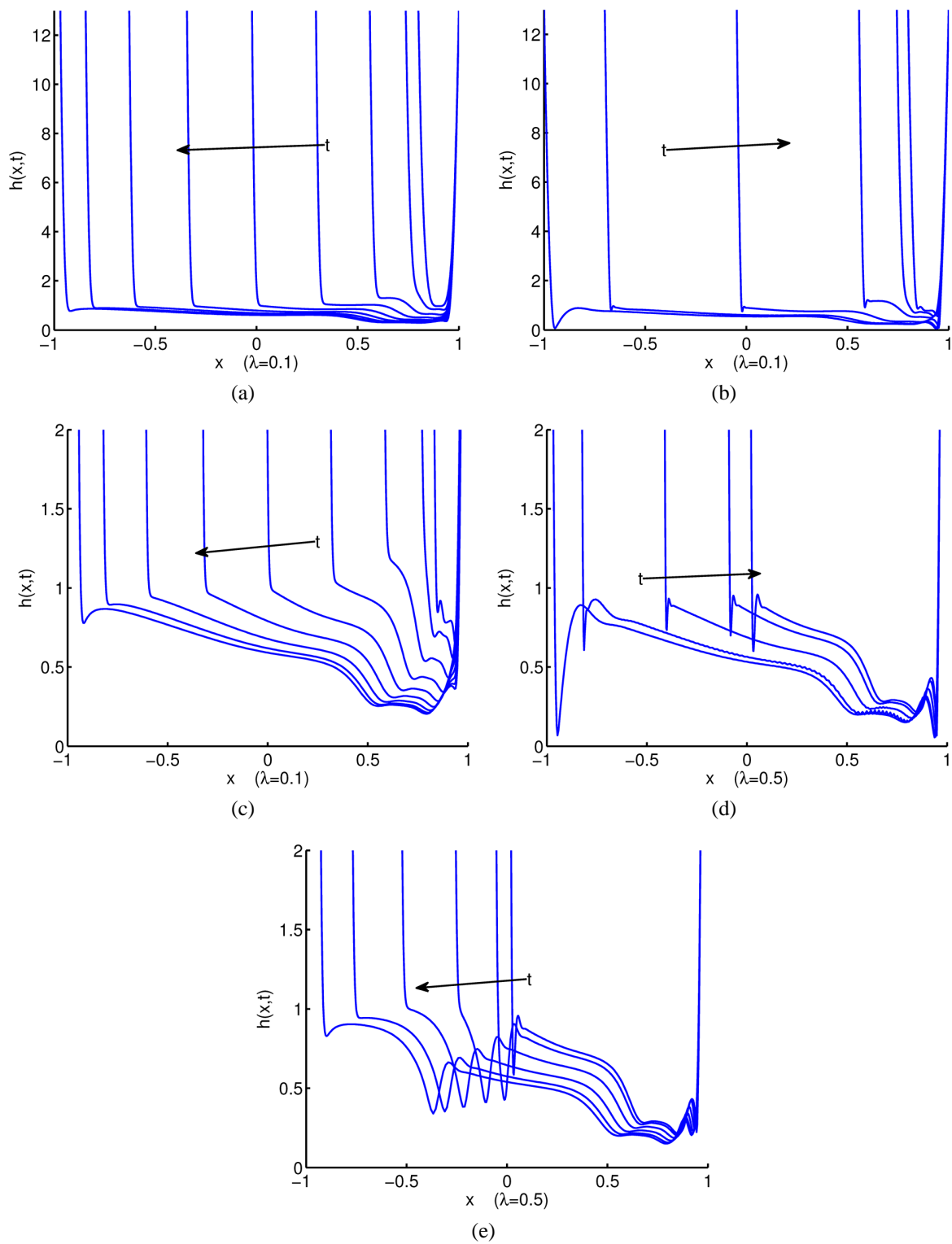
FIG. 5: (**a**) Upstroke of a full blink. (**b**) Downstroke of a full blink. (**c**) Upstroke followed by a half blink. (**d**) Downstroke of a half blink. (**e**) Upstroke of a half blink.
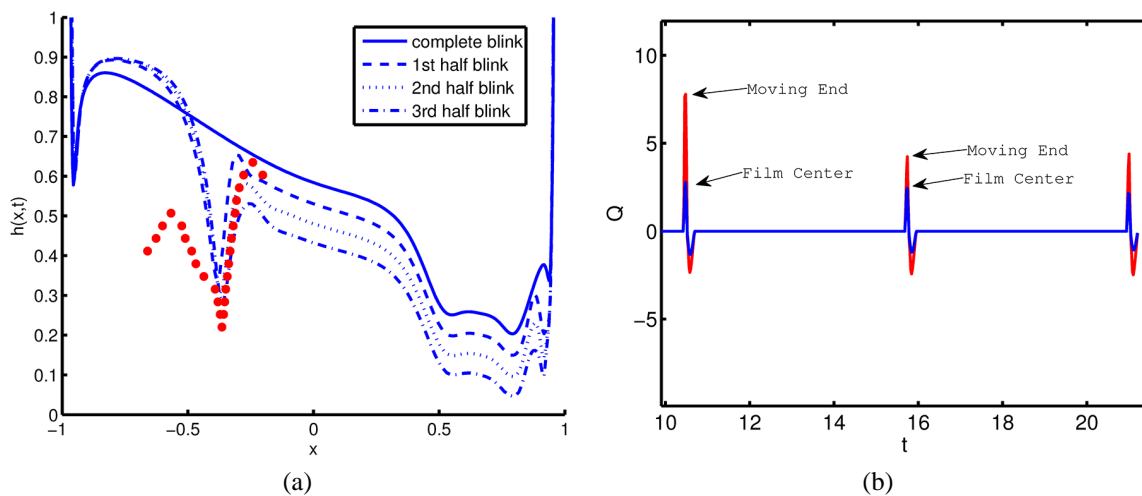
FIG. 6: (**a**) Film thickness profiles at the end of upstrokes of four blinks (three partial blinks following a complete blink). The dots are the experimental observations from Braun and King-Smith (2007) and Heryudono et al. (2007). Parameters used for this computation are $h_e = 1$ (held fixed), and $f_{in} = 0.6$, $r = 0.3$ in FPLM+ condition (28)–(29). (**b**) Fluid flux at both upper meniscus (red) and the middle of the eye (blue) for the three partial blinks.
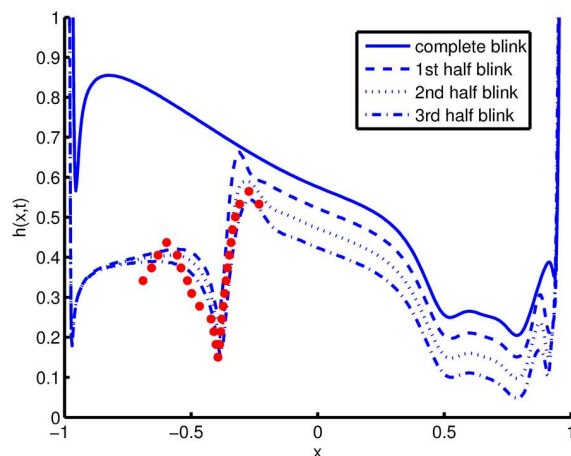
FIG. 7: Film thickness immediately after upstroke phase for several blink cycles with $f_{in} = 0.6$ and $r = 0.3$. Here $h_e = 1$ for the full blink and $h_e = 0.4$ for the subsequent partial blinks.

In Fig. 11, we simulated a partial blink with $\lambda = 0.25$, corresponding to a partial blink that has more corneal coverage than a half blink. Comparing Fig. 11(e) to Fig. 10(e), we observe that the temperature after the blink varies considerably due to the different values of λ, indicating that partial blinks have a strong effect on the corneal temperature for some time range. From Fig. 11(f), we could draw a similar conclusion to that of the half blink case, namely that the temperature variation along the surface relaxes after around 1 s, leaving similar temperature profiles as in Fig. 10(f).

Simulations of corneal temperature reveal that the nonuniformity due to partial blinks disappears rapidly during the interblink. Next we explore the corneal surface temperature and the GCC temperature for the partial blinks, in order to isolate the region that is most affected by blinking parameters and give a quantitative measurement on the average cooling rate.
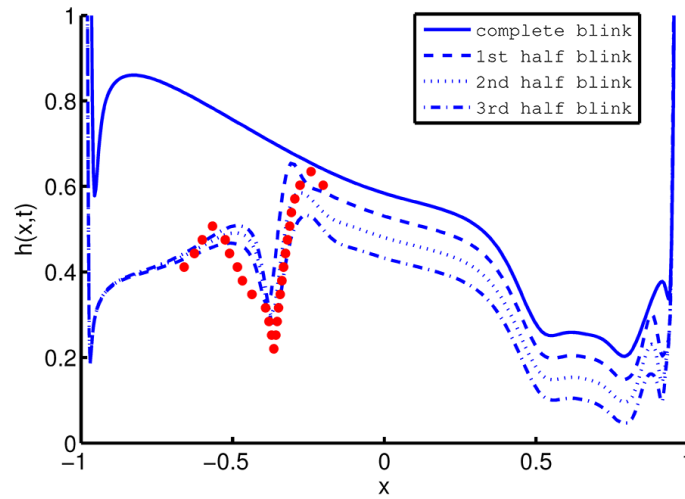
FIG. 8: Film thickness immediately after upstroke phases with $f_{in} = 0.8$ and $r = 0.4$. Here $h_e = 1$ for the full blink and $h_e = 0.4$ for the subsequent partial blinks. The dots are experimental measurements.
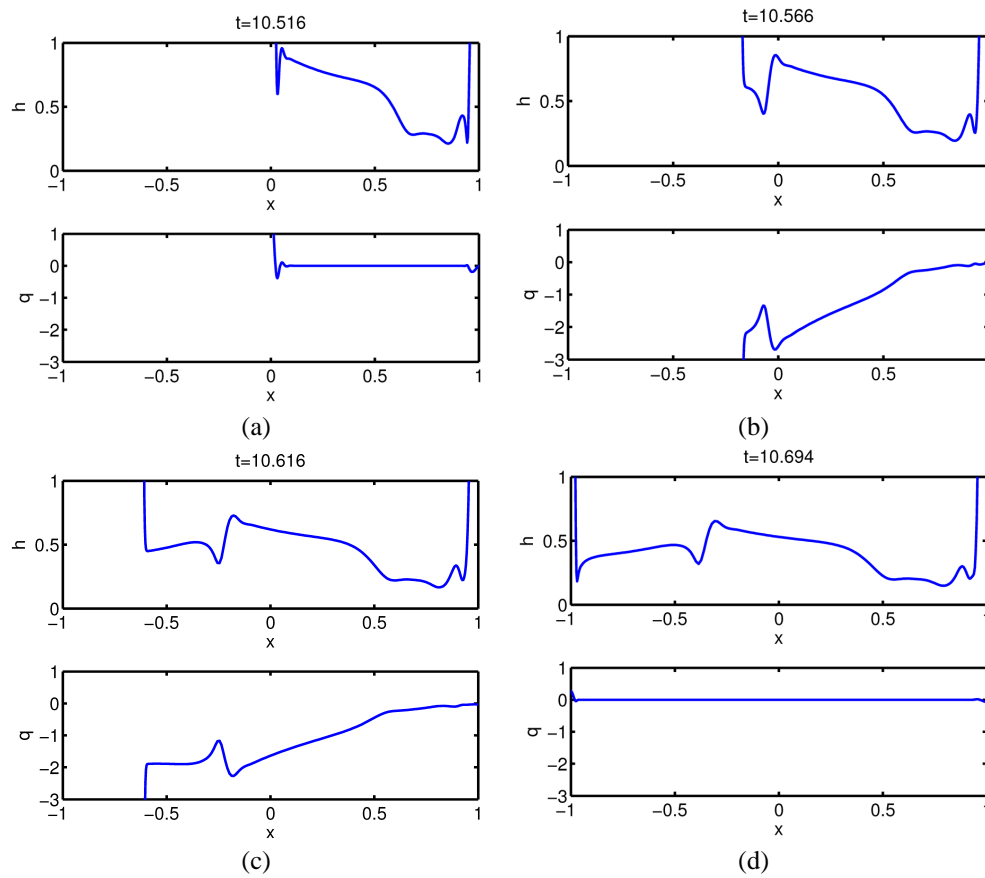
FIG. 9: Film thickness $h(x,t)$ and flux $q(x,t)$ at four consecutive time levels in the upstroke phase of a half blink. Parameters used are $f_{in} = 0.8$ and $r = 0.4$.
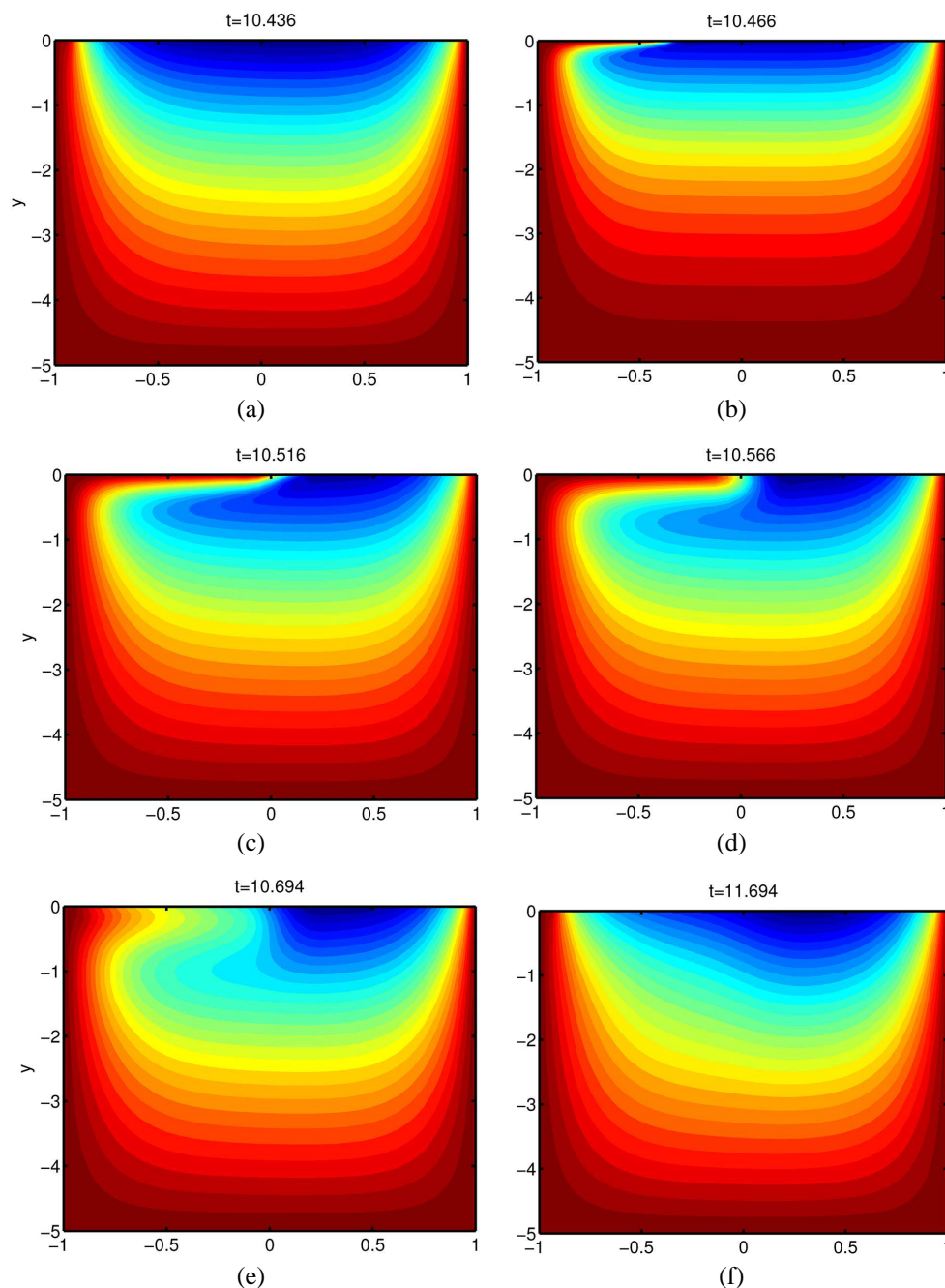
FIG. 10: Temperature dynamics for a complete half blink cycle are shown ($\lambda = 0.5$). The results begin at time $t = 10.436$, after two full interblinks have passed. The domain starts fully open, has closed halfway in (**d**), and in (**f**) the domain is fully open again for 1 s ($t = 11.694$).

Figure 12 shows the GCC temperature comparison between a complete blink and a half blink. In both cases, the temperature drops at a decreasing cooling rate during the interblink, and increases during the downstroke and upstroke, as a result of quick heating from the upper eyelid. It is notable that while the GCC temperature for a full
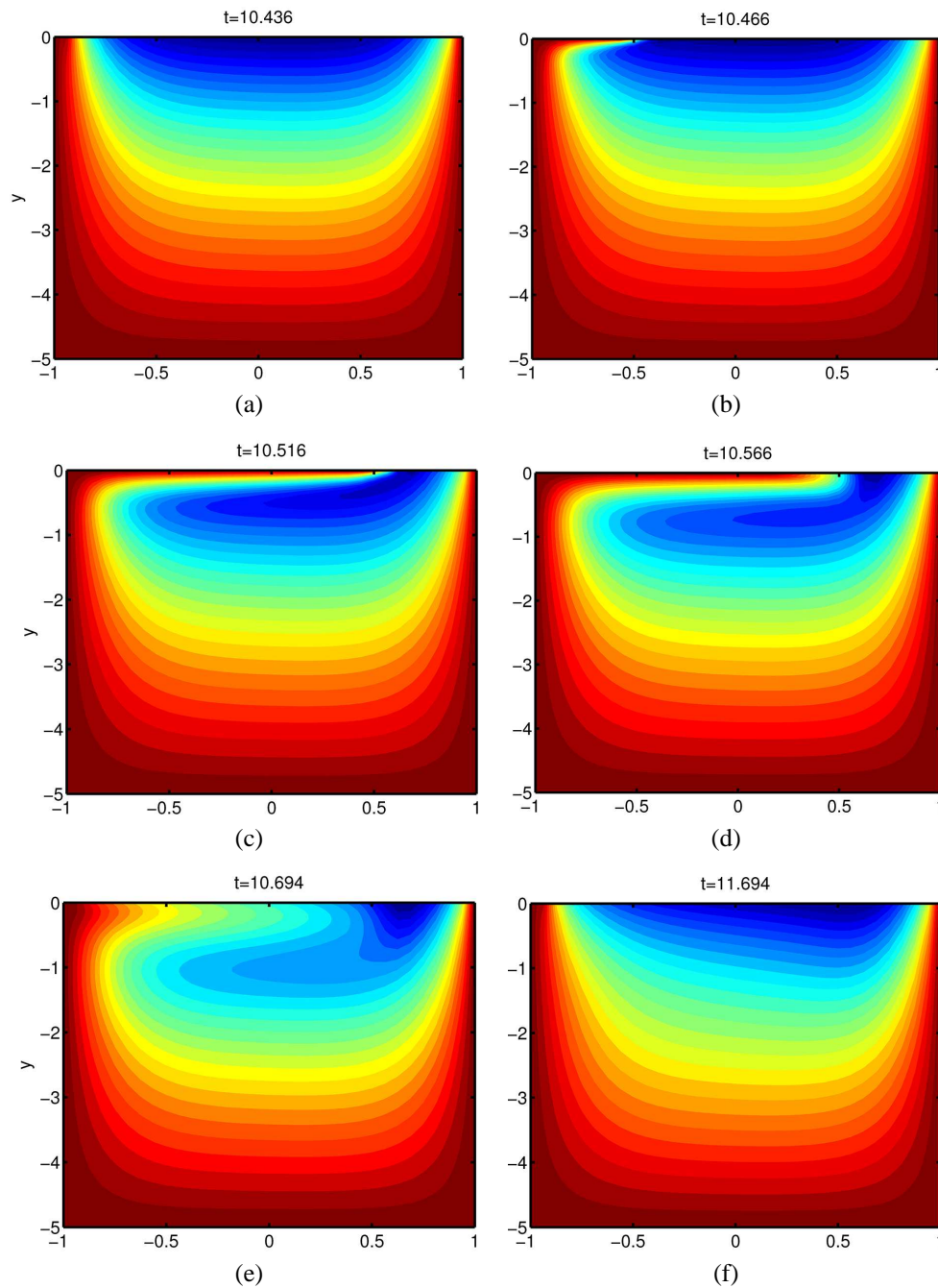
FIG. 11: Temperature dynamics for a complete three-quarter blink cycle are shown ($\lambda = 0.25$). The results begin at time $t = 10.436$, after two full interblinks have passed. The domain starts fully open, has closed halfway in (**d**), and in (**f**) the domain is fully open again for 1 s ($t = 11.694$).

blink remains nearly periodic over multiple blink cycles, there is a noticeable reduction of the peak temperature for each of the half blinks in comparison to the full blinks. Thus, the full blink is essential to maintain consistent function of the eye.

(a)   (b)
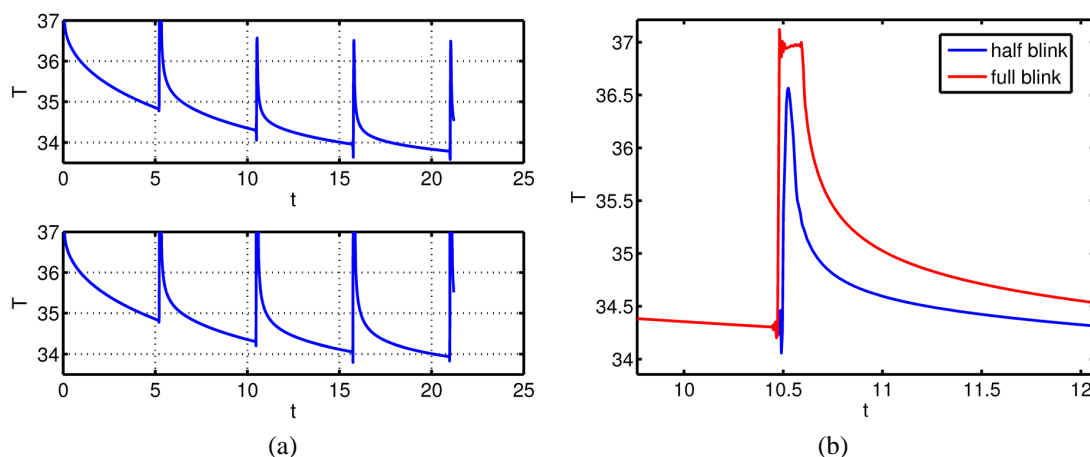
FIG. 12: (**a**) GCC temperature between half blink (top) and complete blink (bottom). For the former, the simulation starts with a full blink followed by three partial blinks. (**b**) Close-up view of same results. All parameters are the same as Fig. 8.

Figure 13 suggests that the nonuniformity at the beginning of the interblink vanishes gradually with increasing time, leaving a greater cooling rate at the superior meniscus than at the inferior meniscus. This suggests that the effect of the temperature difference due to blink behavior on the film dynamics, if it exists, will last less than about 1 s during the interblink. As a result, measuring ocular surface temperature 2 or 3 s after a partial blink should give results quite similar to those of a full blink after the same delay.

4. DISCUSSION AND CONCLUSIONS

In this study we simulated the tear film dynamics for partial blinks coupled with heat diffusion from within the cornea over several blink cycles. We explored this system for realistic lid motion with FPLM+ boundary condition.

(a)   (b)
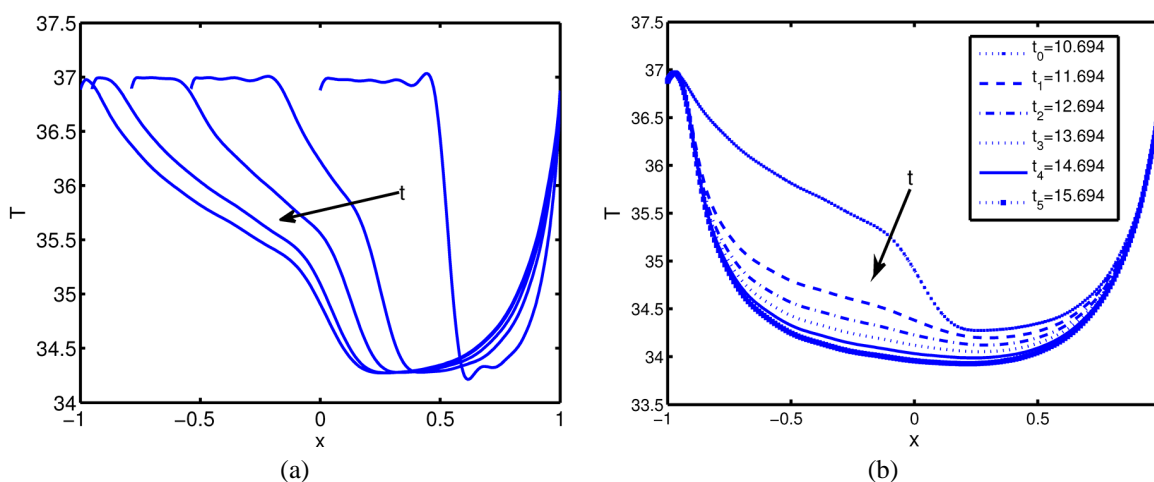
FIG. 13: (**a**) Surface temperature dynamics during the upstroke phase for a half blink with $\lambda = 0.5$. (**b**) Surface temperature dynamics for the interblink after the domain is fully open. All parameters are the same as Fig. 8.

Evaporation was included in the model, so the deformation of the tear film results from the combined effects of capillary thinning and evaporation.

Deng et al. (2013) studied the tear film dynamics for full blink cycles under similar assumptions. They observed how local minima, or black lines, are formed near each end of the film, as have many other studies. They found similar results to Aydemir et al. (2010) and Zubkov (2012) for tear film thickness distribution for full blinks. Our model does not capture the subsequent flow of the tear film in the superior direction after a blink in the early part of the interblink because we use the uniform stretching limit. The other studies have not treated partial blinks.

Braun and King-Smith (2007) and Heryudono et al. (2007) were able to make quantitative comparisons of the thickness distribution left behind after a half blink by using interferometric thickness measurements based on the methods in King-Smith et al. (2006). Their comparisons between the simulated results and the data show that some aspects of the tear film distribution are captured. However, less fluid is stored on the superior side of the valley formed by the partial blink *in vivo* in comparison with the computed results. To improve the model, we revisited the assumption that there is a pre-existing fluid layer under the tear film that has a constant time-independent thickness h_e (Jones et al., 2005). By analyzing the tear flux for partial blink cases, we postulated that the value of h_e should be reduced from complete blink to partial blink.

We compare our simulation with the same *in vivo* data from Braun and King-Smith (2007) and Heryudono et al. (2007), and find that in the new model the simulation not only captures the valley formed due to the half blink but also that less volume remains on the superior side of the valley with a little bump formed near the valley. This improvement was not observed without reducing h_e during the simulation. We note that, as in Braun and King-Smith (2007) and Heryudono et al. (2007), the FPLM+ boundary condition is in some sense a perturbation to the FPLM condition, and that the FPLM+ condition helps contribute to the correct shape of the valley. We did notice a significant contribution from the temperature dynamics to the valley profile in this model.

Thermal dynamics of the tear film, such as GCC temperature, are the other focus of this study. Craig et al. (2000) used ocular thermography, a variety of tear physiology tests, and measurement of evaporation rates in both control and dry eye subjects in order to correlate physiological factors in dry eye with OST and evaporation from the tear film. They found that there was an increased rate of evaporation in dry eye, as found in a number of previous studies (Rolando and Refojo, 1983; Mathers et al., 1993; Mathers, 1993). Dry eye subjects were found to have significantly lower GCC temperature than the controls, and this could be attributed to increased evaporation. Also, the rate of cooling in the cornea was significantly higher in dry eyes, which may be caused by increased evaporation as well. Two studies have found that evaporation can be reduced in dry eye (Fujishima et al., 1996; Mori et al., 1997) but these authors point out that their subjects are aqueous deficient dry eyes, and Craig et al. (2000) speculate that this may be responsible for the reduced evaporation rate. Leiske et al. (2012) and Bron et al. (2004) also showed that the temperature dynamics may have an impact on lipid layer dynamics, for example, which have temperature-dependent properties.

Li and Braun (2012) studied the thermal properties for the interblink phase, where they compared the GCC cooling rate with Efron's measurement (Efron et al., 1989). Deng et al. (2013) extended the comparison to several blink cycles, so they were able to capture the effect of blinking on the temperature dynamics. Though we did not systematically vary the evaporation rate here, we note that for the open eye calculation (Li and Braun, 2012; their Fig. 12), increased thinning due to evaporation caused increased cooling rates, and lower minimum temperatures for the ocular surface. Both works compare well with Efron's measured cooling rates (Efron et al., 1989). In this paper, we explored the temperature profiles during the half blink for both the anterior chamber and the tear film. The simulation reveals that lid motion has significant effect on corneal temperature during the blinking and for a short period after the blink. The distortion in temperature is more severe near the tear film than inside the cornea. This nonuniformity decays relatively rapidly after the eye opens, leaving a more uniform temperature profile during the interblink. This finding shows that the temperature-dependent properties, if they are present, may only be significant during the actual blink or shortly after the blink.

Future directions include incorporating two-dimensional tear films on eye-shaped domains to be solved over three-dimensional regions of heat diffusion that approximate the ocular surface and underlying fluid. Such models could use different properties for the cornea and aqueous humor, as well as for conjunctiva, stroma, and vitreous humor, that are posterior to the tear film. Furthermore, more complex treatments of the tear film, e.g., with separate lipid and aqueous

layers, may add additional insights into tear film and OST dynamics, and the OST may be an important input into the properties of the lipid layer (Leiske et al., 2012).

ACKNOWLEDGMENTS

REFERENCES

Abelson, M. B. and Holly, F. J., A tentative mechanism for inferior punctate keratopathy, *Am. J. Ophthalmol.*, vol. **83**, pp. 866–869, 1977.

Ajaev, V. S., Evolution of dry patches in evaporating liquid films, *Phys. Rev. E*, vol. **72**, p. 031605, 2005a.

Ajaev, V. S., Spreading of thin volatile liquid droplets on uniformly heated surfaces, *J. Fluid Mech.*, vol. **528**, pp. 279–296, 2005b.

Ajaev, V. S. and Homsy, G. M., Steady vapor bubbles in rectangular microchannels, *J. Colloid Interface Sci.*, vol. **240**, pp. 259–271, 2001.

Aydemir, E., Breward, C. J. W., and Witelski, T. P., The effect of polar lipids on tear film dynamics, *Bull. Math. Biol.*, vol. **73**, pp. 1171–1201, 2010.

Berger, R. E. and Corrsin, S., A surface tension gradient mechanism for driving the pre-corneal tear film after a blink, *J. Biomech.*, vol. **7**, pp. 225–238, 1974.

Berke, A. and Mueller, S., The kinetics of lid motion and its effects on the tear film. In: *Lacrimal Gland, Tear Film, and Dry Eye Syndromes 2*, pp. 417–424. Springer, Berlin, 1998.

Berrut, J.-P. and Trefethen, L. N., Barycentric lagrange interpolation, *SIAM Rev.*, vol. **46**, pp. 501–517, 2004.

Braun, R. J., Dynamics of the tear film, *Ann. Rev. Fluid Mech.*, vol. **44**, pp. 267–297, 2012.

Braun, R. J. and Fitt, A. D., Modeling the drainage of the precorneal tear film after a blink, *Math. Med. Biol.*, vol. **20**, pp. 1–28, 2003.

Braun, R. J. and King-Smith, P. E., Model problems for the tear film in a blink cycle: Single equation models, *J. Fluid Mech.*, vol. **586**, pp. 465–490, 2007.

Braun, R. J., Usha, R., McFadden, G. B., Driscoll, T. A., Cook, L. P., and King-Smith, P. E., Thin film dynamics on a prolate spheroid with application to the cornea, *J. Eng. Math.*, vol. **73**, pp. 121–138, 2012.

Bron, A. J., Tiffany, J. M., Gouveia, S. M., Yokoi, N., and Voon, L. W., Functional aspects of the tear film lipid layer, *Exp. Eye Res.*, vol. **78**, pp. 347–360, 2004.

Canning, C. R., Greaney, M. J., Dewynne, J. N., and Fitt, A. D., Fluid ow in the anterior chamber of the eye, *IMA J. Math. Appl. Med. Biol.*, vol. **19**, pp. 31–60, 2002.

Carney, L. G. and Hill, R. M., The nature of normal blinking patterns, *Acta Ophthalmol.*, vol. **60**, pp. 427–433, 1982.

Chen, H.-B., Yamabayashi, S., Ou, B., Tanaka, Y., and Ohno, S., Structure and composition of rat precorneal tear film: A study by in vivo cryofixation, *Invest. Ophthalmol. Vis. Sci.*, vol. **38**, pp. 381–387, 1997.

Craig, J. P., Singh, I., Tomlinson, A., Morgan, P. B., and Efron, N., The role of tear physiology in ocular surface temperature, *Eye*, vol. **14**, pp. 635–641, 2000.

Craster, R. V. and Matar, O. K., Dynamics and stability of thin liquid films, *Rev. Mod. Phys.*, vol. **81**, pp. 1131–1198, 2009.

Cruz, A. A. V., Garcia, D. M., Pinto, C. T., and Cechetti, S. P., Spontaneous eyeblink activity, *Ocul. Surf.*, vol. **9**, pp. 29–30, 2011.

Deng, Q., Braun, R. J., and Driscoll, T. A., Heat transfer and tear film dynamics over multiple blink cycles, 2013 (submitted).

Doane, M. G., Dynamics of the human blink, *Ber. Dtsch. Ophthalmol.*, *Ges*, vol. **77**, pp. 13–17, 1980a.

Doane, M. G., Interactions of eyelids and tears in corneal wetting and the dynamics of the normal human eyeblink, *Am. J. Ophthalmol.*, vol. **89**, pp. 507–516, 1980b.

Doane, M. G., Blinking and the mechanics of the lacrimal drainage system, *Ophthalmol.*, vol. **88**, pp. 844–851, 1981.

Efron, N., Young, G., and Brennan, N. A., Ocular surface temperature, *Curr. Eye Res.*, vol. **8**, pp. 901–906, 1989.

Ehlers, N., The precorneal film: Biomicroscopical, histological and chemical investigations, *Acta Ophthalmol. Suppl.*, vol. **81**, pp. 3–135, 1965.

Fitt, A. D. and Gonzalez, G., Fluid mechanics of the human eye: Aqueous humour flow in the anterior chamber, *Bull. Math. Biol.*, vol. **68**, pp. 53–71, 2006.

Freudenthaler, N., Neuf, H., and Kadner, G., Characteristics of spontaneous eyeblink activity during video display termnial use in healthy volunteers, *Graefes Arch. Clin. Exp. Ophthalmol.*, vol. **241**, pp. 914–920, 2003.

Fujishima, H., Toda, I., Yamada, M., Sato, N., and Tsubota, K., Corneal temperature in patients with dry eye evaluated by infrared radiation thermometry, *Br. J. Ophthalmol.*, vol. **80**, pp. 29–32, 1996.

Gipson, I. K., Distribution of mucins at the ocular surface, *Exp. Eye Res.*, vol. **78**, pp. 379–388, 2004.

Govindarajan, B. and Gipson, I. K., Membrane-tethered mucins have multiple functions on the ocular surface, *Exp. Eye Res.*, vol. **90**, pp. 655–663, 2010.

Harrison, W. W., Begley, C. G., Liu, H., Chen, M., Garcia, M., and Smith, J. A., Menisci and fullness of the blink in dry eye, *Optom. Vis. Sci.*, vol. **85**, pp. 706–714, 2008.

Heryudono, A., Braun, R. J., Driscoll, T. A., Cook, L. P., Maki, K. L., and King-Smith, P. E., Single-equation models for the tear film in a blink cycle: Realistic lid motion, *Math. Med. Biol.*, vol. **24**, pp. 347–377, 2007.

Heys, J. J. and Barocas, V. H., A Boussinesq model of natural convection in the human eye and the formation of Krukenberg's spindle, *Ann. Biomed. Eng.*, vol. **30**, pp. 392–401, 2002.

Himebaugh, N. L., Begley, C. G., Bradley, A., and Wilkinson, J. A., Blinking and tear break-up during four visual tasks, *Optom. Vis. Sci.*, vol. **86**, pp. E106–E114, 2009.

Holly, F. J. and Lemp, M. A., Tear physiology and dry eyes, *Rev. Surv. Ophthalmol.*, vol. **22**, pp. 69–87, 1977.

Johnson, M. E. and Murphy, P. J., Temporal changes in the tear menisci following a blink, *Exp. Eye Res.*, vol. **83**, pp. 517–525, 2006.

Jones, M. B., McElwain, D. L. S., Fulford, G. R., Collins, M. J., and Roberts, A. P., The effect of the lipid layer on tear film behavior, *Bull. Math. Biol.*, vol. **68**, pp. 1355–1381, 2006.

Jones, M. B., Please, C. P., McElwain, D. L. S., Fulford, G. R., Roberts, A. P., and Collins, M. J., Dynamics of tear film deposition and drainage, *Math. Med. Biol.*, vol. **22**, pp. 265–288, 2005.

Jossic, L., Lefevre, P., de Loubens, C., Magnin, A., and Corre, C., The fluid mechanics of shear-thinning tear substitutes, *J. Non-Newton. Fluid Mech.*, vol. **161**, pp. 1–9, 2009.

Karampatzakis, A. and Samaras, T., Numerical model of heat transfer in the human eye with consideration of uid dynamics of the aqueous humour, *Phys. Med. Biol.*, vol. **55**, pp. 5653–5665, 2010.

Kessing, S. V., A new division of the conjunctiva on the basis of x-ray examination, *Acta Ophthalmol.*, vol. **45**, pp. 680–683, 1967.

King-Smith, P. E., Fink, B. A., Fogt, N., Nichols, K. K., Hill, R. M., and Wilson, G. S., The thickness of the human precorneal tear film: Evidence from re ection spectra, *Invest. Ophthalmol.*, *Vis. Sci.*, vol. **41**, pp. 3348–3359, 2000.

King-Smith, P. E., Fink, B. A., Hill, R. M., Koelling, K. W., and Tiffany, J. M., The thickness of the tear film, *Curr. Eye Res.*, vol. **29**, pp. 357–368, 2004.

King-Smith, P. E., Fink, B. A., Nichols, J. J., Nichols, K. K., Braun, R. J., and McFadden, G. B., The contribution of lipid layer movement to tear film thinning and breakup, *Invest. Ophthalmol. Vis. Sci.*, vol. **50**, pp. 2747–2756, 2009.

King-Smith, P. E., Fink, B. A., Nichols, J. J., Nichols, K. K., and Hill, R. M., Interferometric imaging of the full thickness of the precorneal tear film, *J. Opto. Soc. Am. A.*, vol. **23**, pp. 2097–2104, 2006.

Leiske, D. L., Leiske, C. I., Leiske, D. R., Toney, M. F., Senchyna, M., Ketelson, H. A., Meadows, D. L., and Fuller, G. G., Temperature-induced transitions in the structure and interfacial rheology of human meibum, *Biophys. J.*, vol. **102**, pp. 369–376, 2012.

Leiske, D. L., Raju, S. R., Ketelson, H. A., Millar, T. J., and Fuller, G. G., The interfacial viscoelastic properties and structures of human and animal meibomian lipids, *Exp. Eye Res.*, vol. **90**, pp. 598–604, 2010.

Li, L. and Braun, R. J., A model for the human tear film with heating from within the eye, *Phys. Fluids*, vol. **24**, p. 062103, 2012.

Lorber, M., Gross characteristics of normal human lacrimal glands, *Ocul. Surf.*, vol. **5**, pp. 13–22, 2007.

Maki, K. L., Braun, R. J., Driscoll, T. A., and King-Smith, P. E., An overset grid method for the study of reflex tearing, *Math. Med. Bio.*, vol. **25**, pp. 187–214, 2008.

Maki, K. L., Braun, R. J., Henshaw, W. D., and King-Smith, P. E., Tear film dynamics on an eye-shaped domain I: Pressure boundary conditions, *Math. Med. Bio.*, vol. **27**, pp. 227–254, 2010a.

Maki, K. L., Braun, R. J., Ucciferro, P., Henshaw, W. D., and King-Smith, P. E., Tear film dynamics on an eye-shaped domain II: Flux boundary conditions, *J. Fluid Mech.*, vol. **647**, pp. 361–390, 2010b.

Mathers, W. D., Ocular evaporation in meibomian gland dysfunction and dry eye, *Ophthalmol.*, vol. **100**, pp. 347–351, 1993.

Mathers, W. D., Binarao, G., and Petroll, M., Ocular water evaporation and the dry eye: A new measuring device, *Cornea*, vol. **12**, pp. 335–340, 1993.

Maurice, D. M., The dynamics and drainage of tears, *Int. Ophthalmol. Clin.*, vol. **13**, pp. 103–116, 1973.

McCulley, J. P. and Shine, W., A compositional based model for the tear film lipid layer, *Tr. Am. Ophth. Soc.*, vol. **95**, pp. 79–93, 1997.

McDonald, J. E. and Brubaker, S., Meniscus-induced thinning of tear films, *Am. J. Ophthalmol.*, vol. **72**, pp. 139–146, 1971.

McMonnies, C. W., Incomplete blinking: Exposure keratopathy, lid wiper epitheliopathy, dry eye, refractive surgery, and dry contact lenses, *Cont. Lens Anterior Eye*, vol. **30**, pp. 37–51, 2007.

Miller, K. L., Polse, K. A., and Radke, C. J., Black line formation and the perched human tear film, *Curr. Eye Res.*, vol. **25**, pp. 155–162, 2002.

Mishima, S., Some physiological aspects of the precorneal tear film, *Arch. Ophthalmol.*, vol. **73**, pp. 233–241, 1965.

Monster, A. W., Chan, H. C., and O'Connor, D., Long-term trends in human eye blink rate, *Biotelem, Patient Monitor.*, vol. **5**, pp. 206–222, 1978.

Mori, A., Oguchi, Y., Okusawa, Y., Onon, M., Fujishima, H., and Tsubota, K., Use of high-speed, high-resolution thermography to evaluate the tear film layer, *Am. J. Ophthalmol.*, vol. **124**, pp. 729–735, 1997.

Mudgil, P. and Millar, T. J., Adsorption of apo- and holo-tear lipocalin to a bovine meibomian lipid film, *Exp. Eye Res.*, vol. **86**, pp. 622–628, 2008.

Mudgil, P., Torres, M., and Millar, T. J., Adsorption of lysozyme to phospholipid and meibomian lipid monolayer films, *Coll. Surf. B: Biointerfaces*, vol. **48**, pp. 128–137, 2006.

Nagyová, B. and Tiffany, J. M., Components of tears responsible for surface tension, *Curr. Eye Res.*, vol. **19**, pp. 4–11, 1999.

Ng, E. Y. K. and Ooi, E. H., FEM simulation of the eye structure with bioheat analysis, *Comp. Meth. Prog. Biomed.*, vol. **82**, pp. 268–276, 2006.

Ng, E. Y. K. and Ooi, E. H., Ocular surface temperature: A 3D FEM prediction using bioheat equation, *Comp. Biol. Med.*, vol. **37**, pp. 829–835, 2007.

Nichols, J. J., King-Smith, P. E., Hinel, E. A., Thangavelu, M., and Nichols, K. K., The use of fluorescent quenching in studying the contribution of evaporation to tear thinning, *Invest. Ophthal. Vis. Sci.*, vol. **53**, no. 9, pp. 5426–5432, 2012.

Nichols, J. J., Mitchell, G. L., and King-Smith, P. E., Thinning rate of the precorneal and prelens tear films, *Invest. Ophthalmol. Vis. Sci.*, vol. **46**, pp. 2353–2361, 2005.

Nichols, K. K., Nichols, J. J., and Mitchell, G. L., The relation between tear film tests in patients with dry eye disease, *Ophthal. Physiol. Opt.*, vol. **23**, pp. 553–560, 2003.

Norn, M. S., The conjunctival fluid, its height, volume, density of cells, and flow, *Acta Ophthalmol.*, vol. **44**, pp. 212–222, 1966.

Norn, M. S., Semiquantitative interference study of fatty layer of precorneal film, *Acta Ophthalmol.*, vol. **57**, pp. 766–774, 1979.

Ooi, E. H. and Ng, E. Y. K., Simulation of aqueous humor hydrodynamics in human eye heat transfer, *Comp. Biol. Med.*, vol. **38**, pp. 252–262, 2008.

Oron, A., Davis, S. H., and Bankoff, S. G., Long-scale evolution of thin liquid films, *Rev. Mod. Phys.*, vol. **69**, pp. 931–980, 1997.

Owens, H. and Phillips, J., Spread of the tears after a blink: Velocity and stabilization time in healthy eyes, *Cornea*, vol. **20**, pp. 484–487, 2001.

Palakuru, J. R., Wang, J., and Aquavella, J. V., Effect of blinking on tear dynamics, *Invest. Ophthalmol. Vis. Sci.*, vol. **48**, pp. 3032–3037, 2007.

Pandit, J. C., Nagyová, B., Bron, A. J., and Tiffany, J. M., Physical properties of stimulated and unstimulated tears, *Exp. Eye Res.*,

vol. **68**, pp. 247–253, 1999.

Rolando, M. and Refojo, M. F., Tear evaporimeter for measuring water evaporation rate from the tear film under controlled conditions in humans, *Exp. Eye Res.*, vol. **36**, pp. 25–33, 1983.

Scott, J. A., The computation of temperature rises in the human eye induced by infrared radiation, *Phys. Med. Biol.*, vol. **33**, pp. 243–257, 1988a.

Scott, J. A., A fnite element model of heat transport in the human eye, *Phys. Med. Biol.*, vol. **33**, pp. 227–241, 1988b.

Sharma, A., Tiwari, S., Khanna, R., and Tiffany, J. M., Hydrodynamics of meniscus-induced thinning of the tear film. In: *Lacrimal Gland, Tear Film, and Dry Eye Syndromes 2*, pp. 425–431, Springer, Berlin, 1998.

Sibony, P. A. and Evinger, C., Anatomy and physiology of normal and abnormal eyelid position and movement. In: Miller, N., Ed., *Walsh & Hoyt's Clinical Neuro-ophthalmology*, pp. 1509–1592, Williams and Wilkins, Baltimore, 1992.

Tiffany, J. M., The viscosity of human tears, *Intl. Ophthalmol.*, vol. **15**, pp. 371–376, 1991.

Tsubota, K., Tear dynamics and dry eye, *Prog. Retin. Eye Res.*, vol. **17**, pp. 565–596, 1998.

Wang, J., Fonn, D., Simpson, T. L., and Jones, L., Precorneal and pre- and postlens tear film thickness measured indirectly with optical coherence tomography, *Invest. Ophthalmol. Vis. Sci.*, vol. **44**, pp. 2524–2528, 2003.

Winter, K. N., Anderson, D. M., and Braun, R. J., A model for wetting and evaporation of a post-blink precorneal tear film, *Math. Med. Biol.*, vol. **27**, pp. 211–225, 2010.

Wong, H., Fatt, I., and Radke, C. J., Deposition and thinning of the human tear film, *J. Colloi Interface Sci.*, vol. **184**, pp. 44–51, 1996.

Zhang, Y. L., Matar, O. K., and Craster, R. V., Analysis of tear film rupture: Effect of non-newtonian rheology, *J. Colloid Interface Sci.*, vol. **262**, pp. 130–148, 2003.

Zhang, Y. L., Matar, O. K., and Craster, R. V., Rupture analysis of the corneal mucus layer of the tear film, *Mol. Simul.*, vol. **30**, pp. 167–172, 2004.

Zubkov, V., Breward, C., and Gaffney, E., Coupling uid and solute dynamics within the ocular surface tear film: A modelling study of black line osmolarity, *Bull. Math. Biol.*, vol. **74**, no. 9, pp. 2062–2093, 2012.

APPENDIX A: MODEL FORMULATION

The scalings are as follows: $L' = 5$ mm is half the width of palpebral fissure and is used in the x direction; the characteristic thickness of the tear film away from the ends is $d' = 5$ μm and is used in the positive y' direction. Since the cornea thickness is $L'_c = 0.5$ mm, L'_c is used in the negative y' direction. The velocity scale is U'. $\epsilon U'$ is the characteristic speed across the film. The time is scaled by L'/U', the pressure p is made nondimensional with viscous scale $\mu U'/(d'\epsilon^2)$, the evaporation rate J is nondimensionalized with $(kd'L_m)/(T'_B - T'_s)$, and the temperature T is nondimensionalized with $T = (T' - T'_s)/(T'_B - T'_s)$. Here T'_s is the saturation temperature and L_m represents the latent heat of vaporization per unit mass. A detailed definition of parameters and their numerical values is given in Table 2.

The ratio of the length scales for the film, $\epsilon = d'/L' = 10^{-3} \ll 1$, justifies the approach from lubrication theory (Oron et al., 1997; Craster and Matar, 2009). Nondimensionalization of the incompressible Navier-Stokes equations together with the energy equation inside the film leads to the following leading order equations on $X(t) < x < 1$ and $0 \leq y \leq h(x,t)$:

$$\partial_x u + \partial_y v = 0, \quad \partial_y^2 u - \partial_x p + G = 0, \quad \partial_y p = 0, \tag{A1}$$

$$\partial_y^2 T = 0. \tag{A2}$$

The inertial terms in the x component of momentum conservation are proportional to $\epsilon \mathrm{Re}$ where $\mathrm{Re} = \rho U' d/\mu$ is the Reynolds number; using the small value of U', $\mathrm{Re} \approx 1$, but the factor $\epsilon \mathrm{Re}$ is small and we neglect it. The inertial terms in y-component momentum conservation are proportional to $\epsilon^2 \mathrm{Re}$ and the viscous terms are $O(\epsilon^2)$ or smaller. Here $G = (\rho g d^2)/(\mu U')$ is the Stokes number. For typical blink conditions and normal tear film thicknesses, $G \approx 2.5 \times 10^{-3}$. The small Stokes number means that the effect of gravity is prominent only for sufficiently long computations. Since we aim at explaining the effect of partial blinks in one or two complete blink cycles, we will

neglect G in this paper. At the free surface $y = h(x, t)$, interfacial fluid mechanics and evaporation lead to equations in the following nondimensionalized forms:

$$\partial_t h + u\partial_x h + EJ = v, \tag{A3}$$

$$p = -S\partial_x^2 h - A/h^3, \tag{A4}$$

$$\partial_y u = -M\partial_x \Gamma, \tag{A5}$$

$$J + \partial_y T + \text{Bi}(T - T_\infty) = 0, \tag{A6}$$

$$\bar{K}J = \delta p + T. \tag{A7}$$

These equations represent the kinematic condition (A3), the normal (A4) and tangential (A5) stress conditions, the thermal energy balance (A6), and the constitutive equation for the evaporative mass flux (A7). Here $E = k(T'_B - T'_s) / (dL_m \epsilon \rho U')$ is the evaporation constant through the film surface and $S = (\sigma \epsilon^3)/(\mu U') \approx 7 \times 10^{-6}$ is the capillary term. The small value of S means that there will be localized regions of rapid variation near the moving end. $A = A'/(Ld\mu U') \approx 2.1 \times 10^{-6}$ is the nondimensional Hamaker constant in the unretarded van der Waals force. Note that the van der Waals force only becomes significant as film thins to the level near that of the tips of the glycocalyx, and the form we choose prevents film rupture. This combination of evaporation and van der Waals terms has been used to study films (Ajaev and Homsy, 2001), drops (Ajaev, 2005b) and the tear film (Winter et al., 2010). $\Gamma(x, h, t)$ is the surface concentration of a polar component of the lipid layer at the lipid-aqueous surface, which defines the surfactant on the free surface. $M = [\Gamma(\partial\sigma)/(\partial\Gamma)]_0 [\epsilon/(\mu U')] \approx 0.16$ is the Marangoni number representing the change in surface tension relative to viscous effects; the value given is from using blink parameters. This is a significant value for the Marangoni effect that is plausible in comparison with ocular surface observations (Berger and Corrsin, 1974; Owens and Phillips, 2001). The surface concentration of a polar component of the lipid layer at the lipid-aqueous interface is governed by the transport equation

$$\partial_t \Gamma + \partial_x(u^{(s)}\Gamma) - \text{Pe}_s^{-1}\partial_x^2 \Gamma = 0. \tag{A8}$$

Here $u^{(s)}$ is the surface velocity, $\text{Pe}_s^{-1} = D_s/LU'$ is the Péclet number, and D_s is the surface diffusivity of Γ, given by $D_s = 10^{-9}\text{m}^2/\text{s}$. We estimate $\text{Pe}_s^{-1} \approx 2 \times 10^{-6}$, which is small, and the surface diffusion term is neglected. In this paper, we simplify the problem by taking the limit $M \gg 1$, corresponding to a strong Marangoni effect. Following Braun and King-Smith (2007), one obtains the surface velocity

$$u^{(s)} = \dot{X}\frac{1 - x}{1 - X}, \tag{A9}$$

and we refer to this case as the uniform stretching limit.

At $y = 0$, the interface between the tear film and the cornea, we have no-slip and no-penetration conditions for fluid, continuity of temperature, and a time-varying heat transfer condition. Specifically,

$$u = v = 0, \quad T_0 = \tilde{T}, \quad \text{where} \quad T_0 = T(x, 0, t), \tag{A10}$$

$$\partial_{\tilde{y}}\tilde{T}(x, 0, t) + (1 - \psi)\frac{L'_c \tilde{k}}{h_e d}(T_0 - T_B) + \psi\text{Bi}(T_0 - T_\infty) = 0, \quad -1 < x < 1. \tag{A11}$$

Here,

$$\psi(x, t) = \frac{1}{2}\left[1 + \tanh\left(\frac{x - X(t)}{x_w}\right)\right], \tag{A12}$$

is used to smoothly join the the heat diffusion rates from cornea to the open eye and to the upper eyelid (see Fig. 2). Here x_w is a parameter characterizing the width of the transition, typically ranging from 0.1 to 0.01. $\text{Bi} = h_c d'/k$ is the Biot number indicating the ratio of the heat resistance inside of and at the surface of the tear film. We choose $\text{Bi} = 0.0009$ for the simulation, as suggested by Li and Braun (2012).

Here $\tilde{T}$ represents the temperature underneath the film $\tilde{y}_c \leq \tilde{y} \leq 0$, $-1 \leq x \leq 1$, subject to

$$\partial_t \tilde{T} = P_T \left[\left(\frac{L_c'}{L'} \right)^2 \partial_x^2 \tilde{T} + \partial_y^2 \tilde{T} \right], \tag{A13}$$

$$\tilde{T}(x, \tilde{y}_c, t) = \tilde{T}(\pm 1, \tilde{y}, t) = 1, \tag{A14}$$

together with (6). Here $P_T = (L\kappa_c)/(U'L_c^2) \approx 0.76$ is a nondimensionalized heat diffusion rate.

APPENDIX B: FPLM+ CONDITION

Based on the experimental observation of lacrimal gland supply and puncta drainage, we describe the FPLM+ condition (Heryudono et al., 2007) as follows:

$$Q_{\text{top}} = -\dot{X} h_e/2 - f_{\text{out}} Q_p \exp\left[-\left(\frac{t - t_{\text{out}}}{t_p} \right)^2 \right] + f_{\text{in}} Q_{lg} \exp\left[-\left(\frac{t - t_{in}}{t_{lg}} \right)^2 \right], \tag{B1}$$

$$Q_{\text{bot}} = -(1 - f_{\text{out}}) Q_p \exp\left[-\left(\frac{t - t_{\text{out}}}{t_p} \right)^2 \right] + (1 - f_{\text{in}}) Q_{lg} \exp\left[-\left(\frac{t - t_{in}}{t_{lg}} \right)^2 \right]. \tag{B2}$$

Here Q_{lg} represents supply of tear fluid from the lacrimal gland, Q_p represents drainage through the puncta. Detailed derivations of Q_{lg} and Q_p are given later. t_{in} and t_{out} represent the nondimensionalized times at which the influx and the outflux reach their peak values. t_{lg} and t_p specify, respectively, the on-ramp and off-ramp width of the two peaks; they are calculated such that the fluxes match the observation that punctal drainage finished 2 s after the lid opens (Doane, 1981; Maurice, 1973). Nondimensionalization based on L' and U' gives

$$t_{\text{in}} = 0.176, \quad t_{\text{out}} = 1.08, \quad t_{lg} = 0.088, \quad t_p = 0.5, \tag{B3}$$

f_{in} and f_{out} determine the splitting of supply and drainage at the upper and lower lids. Values of $f_{\text{in}} < 1$ allow for some influx from the bottom; this is possible physiologically, as it is observed that there are relatively small lacrimal glands behind the lower lid as well (Lorber, 2007). Typically, $0.65 \leq f_{\text{in}} \leq 0.75$ and $0.5 \leq f_{\text{out}} \leq 0.65$ are used to imply that more supply is through the upper meniscus while drainage is roughly evenly split. We experiment with these parameters further in Sec. 3.

For the lacrimal gland supply, we choose to match the measured steady supply from the lacrimal gland of 1.2 μl/min (Mishima, 1965) and derive the corresponding nondimensional flux $Q_{mT} = 0.01$. To compute Q_{lg}, we need to integrate the Gaussian influx over a complete cycle to balance with the average influx; mathematically,

$$Q_{lg} \int_0^{t_{bc}} e^{-(t-t_{in})^2/(t_{lg})^2} dt = Q_{mT} t_{bc}, \tag{B4}$$

which can be approximated by integrating over the infinite domain as

$$Q_{lg} = \frac{t_{bc}}{\sqrt{\pi} t_{lg}} Q_{mT}. \tag{B5}$$

Based on parameters specified in (B3) we obtain $Q_{lg} = 0.337$. For punctal drainage, we set Q_p such that the net tear influx during each blink compensates the evaporation loss by a factor of r, leading to

$$Q_{mT} t_{bc} - Q_p \int_0^{t_{bc}} e^{-(t-t_{\text{out}})^2/(t_p)^2} dt = r V_e, \tag{B6}$$

where V_e represents the loss of fluid through evaporation at each cycle. The level of compensation for mass lost to evaporation is represented by $0 < r < 1$, with $r = 1$ being full compensation. We can reduce (B6) to

$$Q_p = \frac{Q_{mT}t_{bc} - rV_e}{\sqrt{\pi}t_p}. \tag{B7}$$

Thus the drainage term Q_p depends on the parameter r (see Sec. 3).

In half blink cases, the puncta are assumed to not empty fully and refill during during this period, and the lacrimal gland is assumed to supply a smaller amount of tear fluid. Here we choose $Q_p = 0$ and $Q_{lg} = Q_{lg}/4$ during half blinks, so our flux condition for a half blink is modified from (B1) and (B2), to

$$Q_{\text{top}} = -\dot{X}h_e/2 + f_{\text{in}}\frac{Q_{lg}}{4}\exp\left[-\left(\frac{t - t_{\text{in}} - t_{bc}}{t_{lg}}\right)^2\right], \tag{B8}$$

$$Q_{\text{bot}} = (1 - f_{\text{in}})\frac{Q_{lg}}{4}\exp\left[-\left(\frac{t - t_{\text{in}} - t_{bc}}{t_{lg}}\right)^2\right]. \tag{B9}$$

APPENDIX C: NUMERICAL METHODS

For numerical solution, we transform the domain $X(t) \leq x \leq 1$ to a fixed domain $-1 \leq \xi \leq 1$ via

$$\xi = 1 - 2\frac{1 - x}{1 - X(t)}. \tag{C1}$$

Using the changes of variables $h(x, t) = H[\xi(t), t]$ and $q(x, t) = Q[\xi(t), t]$, we rewrite (1)–(12) to the following:

$$\partial_t H = \frac{1 - \xi}{1 - X}\dot{X}\partial_\xi H - EJ - \left(\frac{2}{1 - X}\right)\partial_\xi Q, \tag{C2}$$

$$Q = \frac{H^3}{12}\left(\frac{2}{1 - X}\right)\partial_\xi\left[S\left(\frac{2}{1 - X}\right)^2\partial_\xi^2 H + AH^{-3}\right] + \dot{X}\frac{1 - \xi}{2}\frac{H}{2}, \tag{C3}$$

$$J = \left\{\frac{T_0 + \text{Bi}T_\infty H}{1 + \text{Bi}H} - \delta\left[S\left(\frac{2}{1 - X}\right)^2\partial_\xi^2 H + AH^{-3}\right]\right\}\left[K + \frac{H}{1 + \text{Bi}H}\right]^{-1}, \tag{C4}$$

$$H(\xi, 0) = H_{\min} + (h_0 - H_{\min})\xi^m, \tag{C5}$$

$$H(\pm 1, t) = h_0, \quad Q(1, t) = -Q_{\text{bot}}, \quad Q(-1, t) = \dot{X}h_0 + Q_{\text{top}}. \tag{C6}$$

Finally, the pressure is introduced as a dependent variable, such that

$$P(\xi, t) = -S\left(\frac{2}{1 - X}\right)^2\partial_\xi^2 H - AH^{-3}, \tag{C7}$$

and the flux may be written as

$$Q = -\frac{H^3}{12}\left(\frac{2}{1 - X}\right)\partial_\xi P + \dot{X}\frac{1 - \xi}{2}\frac{H}{2}. \tag{C8}$$

Substitution for Q in the film equation (C4) and the boundary conditions leads to a system for H and P with Dirichlet conditions on H and Neumann conditions on P. The resulting system for H and P is what we solve numerically.

Those equations are solved an instance of the method of lines using Chebyshev collocation for the spatial discretization. Because of different rates of variation of quantities between the film and in the interior, we used a heterogeneous discretization with 200 nodes in the x direction for the film thickness and a 20×20 grid for the temperature in the anterior eye. In order to compute time derivatives of quantities, we interpolate with spectral accuracy between the two grids at the anterior eye/tear film interface (Berrut and Trefethen, 2004).

The resulting discrete system is differential-algebraic, due to the lack of a time derivative in (C7), and is integrated in time using MATLAB's `ode15s` implementation of variable order backward-differentiation-like methods.